ACS NANO

www.acsnano.org

ARTICLE

Enhanced Triboelectric Nanogenerators Based on MoS_2 Monolayer Nanocomposites Acting as Electron-Acceptor Layers

Chaoxing Wu,[†,∥] Tae Whan Kim,[*,†,∥] Jae Hyeon Park,[†] Haoqun An,[†] Jiajia Shao,[‡] Xiangyu Chen,[‡] and Zhong Lin Wang[*,‡,§]

[†]Department of Electronic and Computer Engineering, Hanyang University, Seoul 04763, Republic of Korea

[‡]Beijing Institute of Nanoenergy and Nanosystems, Chinese Academy of Science, and National Center for Nanoscience and Technology (NCNST), Beijing 100083, People's Republic of China

[§]School of Materials Science and Engineering, Georgia Institute of Technology, Atlanta, Georgia 30332, United States of America

S *Supporting Information*

ABSTRACT: **As one of their major goals, researchers attempting to harvest mechanical energy efficiently have continuously sought ways to integrate mature technologies with cutting-edge designs to enhance the performances of triboelectric nanogenerators (TENGs). In this research, we introduced monolayer molybdenum-disulfide (MoS_2) into the friction layer of a TENG as the triboelectric electron-acceptor layer in an attempt to dramatically enhance its output performance. As a proof of the concept, we fabricated a vertical contact-separation mode TENG containing monolayer MoS_2 as an electron-acceptor layer and found that the TENG exhibited a peak power density as large as 25.7 W/m^2, which is 120 times larger than that of the device without monolayer MoS_2. The mechanisms behind the performance enhancement, which are related to the highly efficient capture of triboelectric electrons in monolayer MoS_2, are discussed in detail. This study indicates that monolayer MoS_2 can be used as a functional material for efficient energy harvesting.**

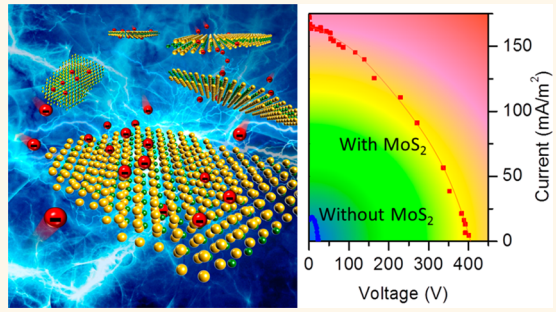

KEYWORDS: *monolayer MoS_2, electron-acceptor, triboelectric nanogenerator, liquid exfoliation, triboelectric enhancement, nanocomposite*

Monolayer molybdenum disulfide (MoS_2), a member of the layered transition-metal dichalcogenide family, is currently being explored and used in high-performance flexible optoelectronics and electronics due to its electrical and optical properties, atomistically thin dimensions, superior high flexibility, and high thermal stability.[1−3] The direct bandgap enables the use of monolayer MoS_2 in high-performance transistors and integrated circuits. Furthermore, the layered MoS_2 and its composites have been used to fabricate light-emitting devices and photodetectors. Its large specific surface area and appropriate energy level, along with the quantum confinement effect, render monolayer MoS_2 a competitive alternative as a charge-trapping material.[4,5] Especially, excellent piezoelectricity and piezotronic effects have been observed in two-dimensional (2D) atomistically thin MoS_2 flakes, which enables mechanical energy to be converted into electricity.[6,7] Note that the piezoelectric output of a MoS_2-based piezoelectric nanogenerator with a power density of 2 mW/m^2 is far from being practical for a power source for a large-scale self-powered wearable electronic device. Recently, triboelectric nanogenerators (TENGs) have been extensively developed to achieve high electricity output, which is due to their high energy-conversion efficiency, to have low cost, simple structure, and flexibility, to be compatible with many materials, and to have the ability to harvest a broad band of mechanical energy from sources such as body motions, vibrations, wind flows, and ocean waves.[8−18] Even though some studies concerning MoS_2-based field-effect transistors driven by TENGs have been performed,[19,20] investigations on the use of monolayer MoS_2 to improve the performance of TENGs have not yet been reported. In this work, in an attempt to enhance dramatically the electrical output performances of TENGs, we fabricated and studied the performance of high-output TENGs employing monolayer MoS_2 as a triboelectric electron-acceptor layer in a negative friction layer.

Received: May 25, 2017
Accepted: July 24, 2017
Published: July 24, 2017

DOI: 10.1021/acsnano.7b03657
ACS Nano XXXX, XXX, XXX−XXX

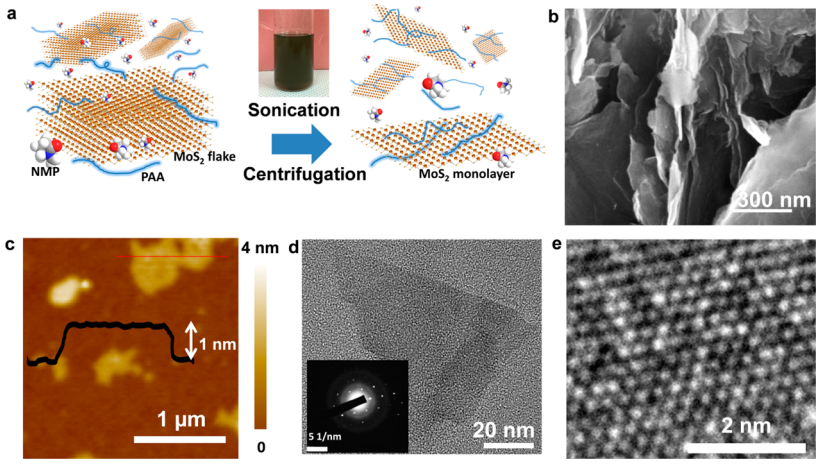

Figure 1. Preparation and characterization of monolayer MoS_2. (a) Schematic illustration of PAA-assisted exfoliation of MoS_2. After MoS_2 flakes had been mixed with a PAA solution, sonication was used to exfoliate the MoS_2 flakes to obtain monolayer MoS_2. The inset presents a photograph of the as-prepared MoS_2 monolayer:PAA suspension. (b) SEM image of the as-prepared MoS_2 monolayer. (c) AFM image and cross-sectional analyses of monolayer MoS_2 deposited on a Si substrate. (d) TEM image of a MoS_2 monolayer; the inset shows the corresponding selected area electron diffraction (SAED) pattern of the MoS_2 sheet. (e) High-magnification TEM image of the MoS_2 monolayer.

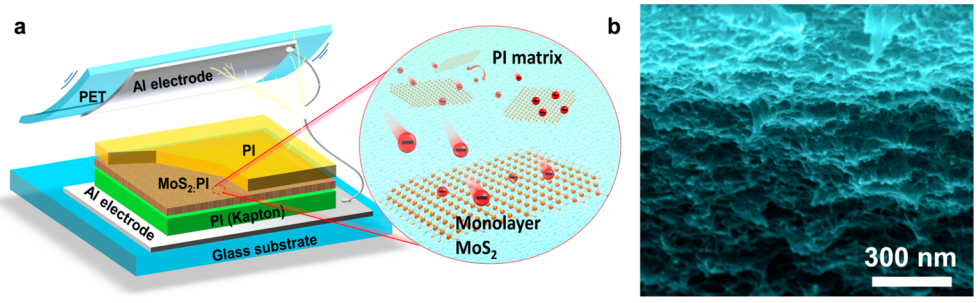

Figure 2. Device structure. (a) Illustration of the vertical contact-separation mode TENG with a MoS_2-monolayer film. The right panel shows a schematic diagram of the electron transfer from the PI layer to the MoS_2 monolayer. (b) Cross-sectional SEM images of the MoS_2:PI layer.

The electrons in the friction layer serve as an electrostatic induction source for the electricity generation process of the TENGs, which has a great impact on the output performances of TENGs. However, once the triboelectric electrons are generated, the electron density on the surface of the friction layer will decrease gradually,[21] and this loss of triboelectric electrons will decrease the potential difference between the two electrodes of the TENGs. To solve this problem, in our previous work, we proposed a methodology for enhancing the output performances of the TENGs by introducing reduced graphene oxide as electron acceptors.[22] Similar to a sheet of reduced graphene oxide, 2D monolayer MoS_2 has a large specific surface area and experiences the quantum confinement effect, thus enabling the realization of electron accepting. Furthermore, the bandgap structure of monolayer MoS_2 allows the TENGs with monolayer MoS_2 to achieve a better performance. We show that the peak power density of TENGs with monolayer MoS_2 is as large as 25.7 W/m^2, which is 120 times larger than that without monolayer MoS_2, and we discuss in detail the performance-enhancement mechanisms relevant to the highly efficient capture of triboelectric electrons in monolayer MoS_2.

RESULTS AND DISCUSSION

The ability to produce monolayer MoS_2 is a critical step toward allowing its implemenation in electronic devices. Liquid-phase exfoliation of bulk MoS_2 powders in organic solvent with the aid of ultrasonication is considered as a viable route to achieve this goal.[23] Here, we used polyamide acid (PAA), a precursor of polyimide (PI), to assist the exfoliation and the dispersion of monolayer MoS_2 from its bulk material in *N*-methyl-2-pyrrolidone (NMP) under sonication. The preparation of the monolayer MoS_2:PAA composite precursor *via* the polymer-assisted exfoliation process is schematically shown in Figure 1a. This suspension was stable under ambient conditions. Good dispersion of MoS_2:PAA in NMP is extremely desirable for device fabrication *via* solution processing and allows the MoS_2:PI layer to be conveniently fabricated by using spin-coating and subsequent imidization,[24] leading to the easy fabrication of TENGs.

The MoS_2 powder was successfully exfoliated into individual nanosheets during the sonication, as shown in Figure 1b. The morphology of the MoS_2 was further studied by using atom force microscopy (AFM). For the AFM measurements, the MoS_2 was prepared from the supernatant *via* repeated washing and centrifugation steps, and then, it was redispersed in NMP and deposited on a Si substrate. Figure 1c shows the AFM image and cross-sectional analysis of the exfoliated MoS_2 nanosheets. The thickness of an obtained MoS_2 nanosheet with a width of a few hundred nanometers was approximately 1 nm. The morphology of the as-prepared MoS_2 was verified by using transmission electron microscopy (TEM) (Figure 1d).

DOI: 10.1021/acsnano.7b03657
ACS Nano XXXX, XXX, XXX−XXX

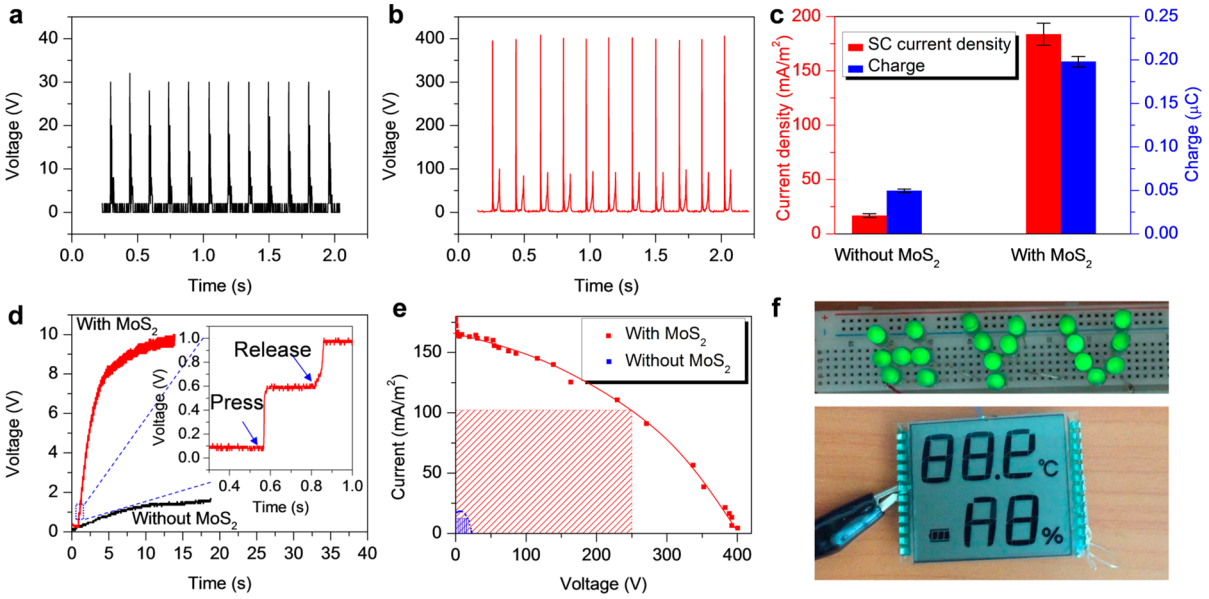

Figure 3. Performances of the TENGs. (a) Rectified open-circuit voltage of the TENG without MoS_2. (b) Rectified open-circuit voltage of the TENG with monolayer MoS_2. (c) Short-circuit current density and the amount of charge generated during a press-release cycle for the TENGs with and without monolayer MoS_2. (d) Charging processes by using the TENGs. The inset is a detailed enlarged view. (e) Curves of the output peak current as a function of the output peak voltage for the TENGs with and without monolayer MoS_2. The area of the largest rectangle defined by the current−voltage curve corresponds to the maximum peak power density. (f) Photographs of green LEDs and a LCD panel directly driven by the TENG with monolayer MoS_2.

The selected area electron diffraction (SAED) pattern shown in the inset of Figure 1d indicates the MoS_2 has hexagonal symmetry, with individual sheets consisting of a single crystal domain.[25] The high-magnification TEM image shown in Figure 1e clearly reveals the honeycomb structure of MoS_2, which confirms that the great majority of the exfoliated sheets are monolayers.[23,26] Note that the apparent thickness of the thin film in the AFM image shown in Figure 1c is a little larger than the values of 0.65−0.7 nm reported for mechanically exfoliated MoS_2 monolayers.[27] This difference may be explained by surface corrugation due to distortion of the MoS_2 layer, the presence of residual PAA molecules, and the presence of a gap between the MoS_2 layer and the substrate. Note that the large specific surface area of 2D materials plays an important role in efficient electron capture; thus, the as-prepared monolayer MoS_2 can allow maximum contact between the MoS_2 and the PI.

A schematic view of a vertical contact-separation mode TENGs based on the MoS_2:PI layer is shown in Figure 2a. The bottom part of the device is made of the glass substrate onto which an Al electrode and a negative friction layer with a PI (Kapton)/MoS_2:PI/PI stacked structure are deposited. The top part of the TENGs is made of a polyethylene terephthalate (PET) substrate onto which an Al electrode is deposited. The top PI layer in the friction layer acts as the negative friction material and can drag electrons from the top Al electrode during the triboelectrification process. The monolayer MoS_2 sheets embedded into the PI layer act as the triboelectric electron acceptors. After the spin-coating and the subsequent imidization, an uniform MoS_2:PI layer can be fabricated, as shown in cross-sectional SEM of the monolayer MoS_2:PI layer in Figure 2b. As a comparison, a TENG without monolayer MoS_2 was fabricated with a friction layer structure of PI (Kapton)film/PI film to investigate and emphasize the effect of the insertion of the monolayer MoS_2 on TENGs' performances. The different devices shared a positive friction layer part for the purpose of facilitating a comparison between the device performances of the TENGs with and without monolayer MoS_2. The fundamental electricity generation mechanisms of typical contact-separation mode TENGs are as follows: Under external forces, a physical contact is initiated between the PI (Kapton)/MoS_2:PI/PI stacked layer and the top Al electrode. The the PI layer accepts electrons due to their different abilities to attract electrons. Once the external forces are released, the top Al electrode separates from the friction layer. Then, the electrostatic balance is broken, and the positive charges in the top Al electrode are driven to the bottom electrode through an external circuit to re-achieve a balance of electrostatic charge. Once the top Al electrode moves back to the friction layer due to the external forces, the positive charges in the bottom electrode move to the top electrode so as to re-achieve the original electrostatic balance. The TENG can be operated cycle-by-cycle by driving it with repeated external forces. In this way, mechanical movements are converted into electricity.

The rectified open-circuit voltages of the TENGs without and with monolayer MoS_2 are shown in Figure 3a and 3b, respectively. The open-circuit voltage of the TENG without MoS_2 is about 30 V (Figure 3a). However, the open-circuit voltage of the optimized TENG with monolayer MoS_2 is as high as 400 V. Furthermore, the short-circuit (SC) current density of the TENG with monolayer MoS_2 is obviously higher than that of the TENG without MoS_2, as shown in Figure 3c. Note that the electricity generated by using TENGs needs to be stored in an energy-storage device before powering electronic devices. Thus, the total amount of charge, rather than the peak current, is the key to the efficient charging of an energy-storage device. The total amount of charge generated by a press-release cycle for a TENG with monolayer MoS_2 reached approximately 0.2 μC, which was much larger than that (0.05 μC) produced by using a TENG without MoS_2, as shown in Figure 3c.

DOI: 10.1021/acsnano.7b03657
ACS Nano XXXX, XXX, XXX−XXX

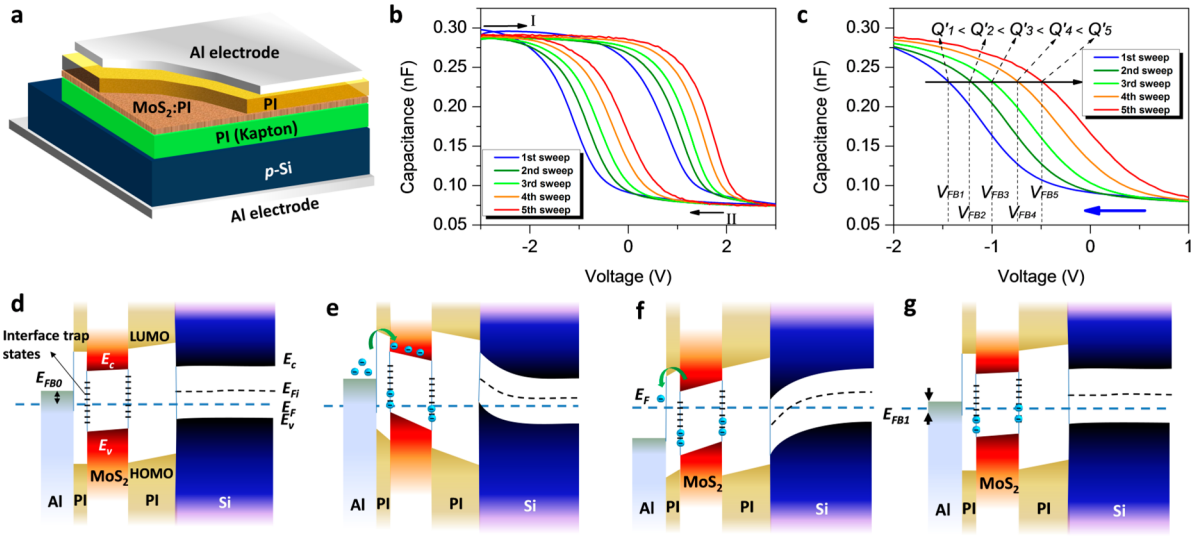

Figure 4. Analyses of the electron-trapping mechanisms. (a) Illustration of the floating-gate MIS device used for the *C*−*V* measurements. (b) *C*−*V* curves of the floating-gate MIS device as the applied voltage was swept from −3 to 3 V and from 3 to −3 V. (c) Detailed *C*−*V* curves during the voltage sweep from 3 to −3 V. The V_{FB} can be seen to shift toward higher voltage, and the density of captured charge, Q', can be seen to increase with increasing number of voltage sweeps. (d–g) Schematic diagrams of the energy bands for the floating-gate MIS device. (d) A negative voltage (V_{FB0}) is applied to keep the device in a flat-band state. (e) When a larger negative voltage is applied, the injected electrons are captured in the MoS_2 monolayer. (f) When a larger negative voltage is applied, some of the captured electrons are released from the MoS_2 monolayer. (g) A smaller negative voltage (V_{FB1}) is applied to keep the device in a flat-band state due to the capture of electrons in the insulator layer.

A 0.22 μF capacitor was charged by using a TENG with monolayer MoS_2, as shown in Figure 3d. The capacitor was charged to 10 V in merely 15 s, which is a gigantic enhancement compared to the performance of the TENG without MoS_2. The inset of Figure 3d shows an enlarged view of the details. Both the press and the release operations can charge the capacitor because of the rectification of the output signals. The voltage of the charged capacitor can be increased by 0.5 V in each press process by using the TENG with monolayer MoS_2. However, each press or release process can only result in a voltage increase of about 0.1 V for a TENG without MoS_2.

The curves for the output peak current as a function of the output peak voltage for the TENG with monolayer MoS_2 and for the TENG without MoS_2 were characterized, and the results are shown in Figure 3e. The area of the largest rectangle defined by the current−voltage curve determines the maximum peak power density. The TENG with monolayer MoS_2 reached a maximum peak power density value of 25.7 W/m^2 at a resistance of approximately 5 MΩ, which is 120 times larger than that of the TENG without MoS_2. Furthermore, Figure 3f shows that the TENG with monolayer MoS_2 could serve as a direct power source for a commercial multicolor light-emitting diode (LED) array (in series) and for a liquid-crystal display (LCD) panel. The TENG, which was triggered by pressing and releasing, generated current pulses that instantaneously lit a LED array and a LCD panel, as shown in Video S1 and Video S2 of the Supporting Information.

It is worth noting that the voltage generated under open-circuit conditions is proportional to the electron density (σ) as follows:

$$V = \frac{\sigma \times x(t)}{\varepsilon} \quad (1)$$

where V is the open-circuit voltage, $x(t)$ is the gap between the electrodes at time t, and ε is the permittivity.[28] As a result, the performance can be enhanced by increasing the density of triboelectric electrons. We attribute the mechanism for the dramatic increase in the electrical output of the TENG with monolayer MoS_2 to efficient electron capture in the monolayer MoS_2, which can suppress the process causing the loss of the as-generated triboelectric electrons.

Among the several processes causing the loss of triboelectric electrons, in a contact-separation-triggered TENG, air breakdown is likely to happen between the two triboelectric surfaces with opposite static charges due to the high voltage created in the vertical separation process.[29,30] The drift process caused by the electric field and the diffusion process engendered by the concentration gradient of the electrons can also result in the loss of triboelectric electrons because of recombination with positive charges induced on the electrode. Furthermore, the loss of triboelectric electrons can come from adsorbing positively charged ions or particles from the air, and the adsorbed positive charges can then recombine with triboelectric electrons on the surface.[21] Here, we introduce electron acceptors in the negative friction layer, in which monolayer MoS_2 acts as electron acceptors. The monolayer MoS_2 can efficiently capture most of the as-generated triboelectric electrons due to its high electron-capture properties and large specific surface areas.[4,5] In other word, the as-generated triboelectric electrons on the surface of the PI might be transferred into the MoS_2 layer embedded in the PI layer and stored inside the negative friction layer rather than on the surface of the negative friction layer. As a result, the static electron density on the negative triboelectric surfaces is decreased, and the gap between the positive and the negative charges is increased, which can weaken the air breakdown effect. The drift and the diffusion effects can also be suppressed due to the high electron-capture properties of monolayer MoS_2.

DOI: 10.1021/acsnano.7b03657
ACS Nano XXXX, XXX, XXX−XXX

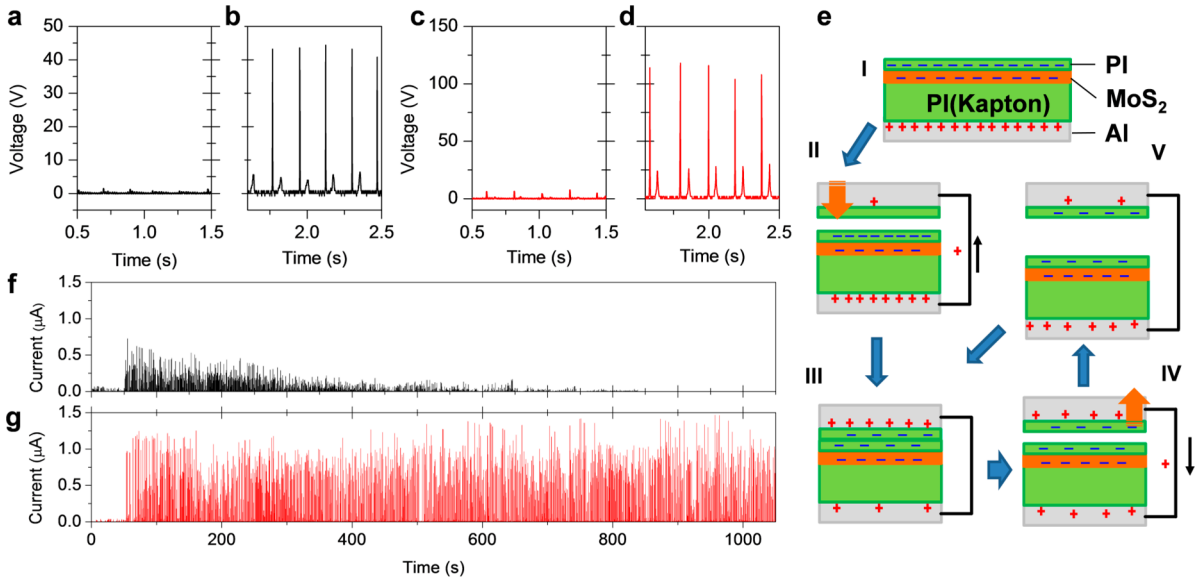

Figure 5. Electron-trapping verification. The structure of the top part of the TENG is PET/Al/PI. Open-circuit output voltage of the devices without MoS_2 (a) before and (b) after surface charging. Open-circuit output voltage of the devices with monolayer MoS_2 (c) before and (d) after surface charging. (e) The working mechanisms of the device. The short-circuit current as a function of the time for the devices (f) without MoS_2 and (g) with monolayer MoS_2.

The outermost region of the PI layer stops the electrons stored in the friction layer and the positive charges adsorbed on the friction layer's surface from coming into contact and can suppress recombination between the triboelectric electrons and the positive charges.

To prove experimentally the existence of electrons trapped in monolayer MoS_2, we fabricated a floating-gate metal-insulator-semiconductor (MIS) device, in which the monolayer MoS_2 layer was used as a charge-storage region in the middle of the PI insulator layer. A schematic diagram of the fabricated floating-gate MIS device with an Al/p-Si/PI/MoS_2:PI/PI/Al structure is shown in Figure 4a. The effect of trapping charge carriers in the monolayer MoS_2 can be directly detected by measuring the capacitance of the MIS device; thus, the capacitance−voltage (C−V) curves for the device were measured at 1 MHz to investigate its electrical characteristics. The C−V measurements were conducted by applying dual voltage sweeps from −3 to 3 V. As shown in Figure 4b, a clockwise hysteresis is clearly observed during the first voltage sweep, which is similar to that of a typical p-Si-based MIS device with charge-trapping regions, indicative of the existence of sites occupied by carriers.[31] The presence of such sites is attributed to the electron-trapping effect of the monolayer MoS_2 embedded in the PI layer. The electrons under negative bias voltages emitted from the top Al electrode are captured in the monolayer MoS_2 contained in the insulator layer.[32] The electrons captured under positive bias voltages are released to the top electrode. A very interesting observation is that all of the C−V curves during the ensuing voltage sweeps shift toward higher voltage, as shown in Figure 4b, which is different from the C−V characteristics of floating-gate MIS devices in which the electron-trapping sites are located in a reduced graphene oxide sheet.[22] The detailed C−V curves during the voltage sweep from 3 to −3 V are presented in Figure 4c. The magnitude of the V_{FB} is significantly related to the number of carriers trapped in the insulator layer. The charge density Q' of the charge captured in the monolayer MoS_2 can be estimated from the following equation:

$$Q' = \frac{\Delta V_{FB} \times d_0 \times C_0}{x} \quad (2)$$

where ΔV_{FB} is the flat-band shift in the C−V curves, d_0 is the thickness of the active layer, C_0 is the capacitance of the dielectric stack layer, and x is the location of the MoS_2 layer.[33] This phenomenon shows that the electrons captured in monolayer MoS_2 cannot be completely released under positive voltages and that the number of electrons captured in monolayer MoS_2 gradually increases with increasing number of voltage sweeps.

Schematic diagrams of the energy bands for the floating-gate MIS device are described in Figure 4d and 4e to explain qualitatively the observed C−V characteristics. First, when a V_{FB} with a negative value is applied to the top electrode, the device maintains a flat-band state (Figure 4d). In this case, no electrons are trapped in the MoS_2 layer. When larger negative applied voltages are applied to the top Al electrode, electrons are injected from the Fermi level of the Al electrode to the lowest unoccupied molecular orbital (LUMO) of the PI and are then captured in the monolayer MoS_2 (Figure 4e). The capture of electrons in the monolayer MoS_2 may cause an accumulation of holes in the PI/p-Si interface, resulting in an increase in the value of the capacitance. The capture of electrons in the monolayer MoS_2 and the ensuing induction of positive-charge accumulation in the floating-gate MIS device are similar to the operating mechanisms of a TENG with electron-trapping sites. The captured electrons can occupy both energy states at the bottom of the conduction band and the trap states of the MoS_2 in the interface. Because the intrinsic bandgap energy of monolayer MoS_2 is as large as 1.8 eV, which is different from that of reduced graphene oxide,[34] the interface trap states are distributed in the band gap. Of note is that for the Fermi−Dirac distribution, the probability of electrons occupying an energy level becomes higher for energy levels below the Fermi level, but tends to decrease dramatically for levels above the Fermi level.[35] Under positive voltages, the electrons in energy states at the bottom of the conduction band might be released to the

DOI: 10.1021/acsnano.7b03657
ACS Nano XXXX, XXX, XXX−XXX

top electrode, while those in the band gap tend to be captured in interface traps, as shown in Figure 4f. As a result, a smaller V_{FB} is needed to obtain the flat-band condition (Figure 4g). When the number of voltage sweeps increases, the number of electrons captured in the interface trap states of the MoS_2 gradually increases, leading to a shift in the $C-V$ curves.

To further verify the important role of the electron acceptors in the performance of TENGs, we designed an experimental setup to monitor charge transfers. Two kinds of TENGs, one with a bottom part of PI (Kapton)/MoS_2:PI/PI and the other with a bottom part of PI (Kapton)/PI, were prepared. The top parts of the two kinds of TENG were the same and were made of PET/Al/PI. The active area of the TENG was 1.5 cm × 2.5 cm. Additional triboelectric charges cannot be generated during the contact process due to the same electron-gaining ability of the PI. Initially, no efficient electricity output was observed for either device during the press-release processes due to the friction materials having the same electron-gaining ability, as shown in Figure 5a and Figure 5c. We should note that the devices had a small electricity output during the initial stage, which might have resulted from a small number of interface charges or absorbed charges introduced during the fabrication process.

The triboelectric electrons in the bottom part of the TENG were introduced by rubbing the bottom part of the TENG with an Al foil. The device with monolayer MoS_2 showed an open-circuit voltage of approximate 120 V (Figure 5d), which was much larger that of the device without MoS_2 (Figure 5b). Some of the surface electrons for the device with monolayer MoS_2 acceptors were transferred into the MoS_2 layer, as shown in Figure 5e-I. Positive charges in the bottom electrode gradually transferred to the top electrode as the top part was closing toward the bottom part (Figure 5e-II). In a contact state, some of the electrons in the bottom part may transfer to the top part due to the same electron-gaining ability, as shown in Figure 5e-III. The bottom part of the device holds a much larger number of electrons than the top part does because of electrons are stored in the MoS_2. As a result, positive charges in the top electrode gradually transfer to the bottom electrode during the separating process, as shown in Figure 5e-IV and 5e-V. A similar phenomenon is seen for the device without MoS_2; the electrons in the bottom part transfer to the top part in a contact state. However, more electrons should transfer to the top part due to the absence of electron acceptors in the bottom part. As a result, the open-circuit voltage of the device without monolayer MoS_2 is smaller than that of the device with monolayer MoS_2.

The short-circuit currents as functions of time at a frequency of 5 Hz are presented in Figure 5f and Figure 5g for the devices without and with monolayer MoS_2, respectively. The output current for the device without MoS_2 is seen to decrease gradually, which may result from discharging effects, including drift, diffusion, and charge recombination. In contrast, the retention test of the device with monolayer MoS_2 demonstrates its higher stability, which further confirms that the introduction of monolayer MoS_2 can suppress the processes through which triboelectric electrons are lost.

CONCLUSIONS

In summary, we have demonstrated that the liquid-phase exfoliated monolayer MoS_2 can act as triboelectric electron acceptors in TENGs, dramatically enhancing their electricity output. That significant increase in the electricity output of the TENGs can be attributed to efficient electron capture in the monolayer MoS_2, which can suppress recombination between triboelectric electrons and positive charges. The maximum power density of vertical contact-separation mode TENGs with monolayer MoS_2 reached 25.7 W/m^2, which is 120 times as large as that of the device without MoS_2. The observations made in this research should provide direction to a frontier in active material selection and device structure design for high-efficiency triboelectric devices. Nanomaterials, including zero-dimensional, one-dimensional, two-dimensional, and three-dimensional nanostructures, and their composites, should be considered for use to provide electron-trapping sites in TENGs.

METHODS

Preparation of the Monolayer MoS_2:PAA Suspension. The PAA solution was prepared by dissolving polyamic acid in NMP and consisted of 287.5 mg of *p*-phenylenediamine (PDA) and 781.25 mg of biphenyltetracarboxylic dianhydride (BPDA) dissolved in 500 mL of NMP solvent. For the preparation of the monolayer MoS_2:PAA suspension, 10 mg of MoS_2 powder was added to 20 mL of the PAA solution, after which the mixture was sonicated for 9 h. The as-produced suspension was allowed to settle for 7 days under ambient conditions in order to remove any residual particles. Finally, the supernatant was collected for further centrifugation at 4000 rpm for 30 min. The resulting clear colloid was used for the subsequent characterization and device fabrication.

Fabrication of Devices. To fabricate the negative friction layer of the TENG with monolayer MoS_2, we deposited an Al film, acting as an electrode, on the surface of the glass substrate by using thermal evaporation. The MoS_2:PAA film was deposited on the surface of the PI (Kapton) film by using the spin-coating method and was baked at 135 °C for 30 min to evaporate the solvent. Then, another PAA layer was spin-coated onto the surface of the as-prepared MoS_2:PAA layer. After it had been baked at 400 °C for 2 h, the PI (Kapton, 76-μm thick)/MoS_2:PI(1.5-μm thick)/PI(100 nm thick) stacked layer adhered to the surface of the as-fabricated Al electrode. As a comparison, a TENG without MoS_2 was fabricated with a friction layer structure of the PI (Kapton)film/PI film. Briefly, the PI layer was deposited on the PI(Kapton) film by using the same spin-coating method. Note that the thickness of the PI (Kapton) film/PI stacking layer was the same as that of the PI (Kapton)/MoS_2:PI/PI stacking layer for the purpose of facilitating comparisons. The positive friction layer was composed of the PET substrate with a piece of Al foil affixed to its surface. The positive friction layer for the vertical contact-separation mode TENG was supported by a spring with a thickness of 10 mm, which served as a spacer for the TENG. The active area of the TENG was 1.5 cm × 2.5 cm. The different negative friction layers used in this work shared a positive friction layer for the purpose of facilitating comparisons.

A floating-gate MIS device with a structure of Al/p-Si/PI(100 nm)/MoS_2:PI(100 nm)/PI(100 nm)/Al was fabricated on the p-Si substrate by using the same spin-coating method. Finally, the top Al electrode pad with a diameter of 0.5 mm was deposited on the PI layer by using thermal evaporation.

Characterization and Electrical Measurements. SEM (FEI, NOVA nanoSEM 450) was used to investigate the microtopography of the as-prepared nanomaterials. AFM (Park systems, XE-100) and TEM (JEOL, JEM-2100F) were used to characterize the as-fabricated MoS_2. An oscilloscope (Tektronix, TDS2024C) and a current meter (Keithley, 2400) were used for measuring the electricity output of the TENGs. The $C-V$ curves were measured using a Keithley 4200SCS unit.

ASSOCIATED CONTENT

Supporting Information

The Supporting Information is available free of charge on the ACS Publications website at DOI: 10.1021/acsnano.7b03657.

DOI: 10.1021/acsnano.7b03657
ACS Nano XXXX, XXX, XXX−XXX

MoS_2-based TENG for directly lighting up tens of green LEDs (AVI)
MoS_2-based TENG for directly lighting up tens of green LCD panel (AVI)

AUTHOR INFORMATION

Corresponding Authors

*E-mail: twk@hanyang.ac.kr.
*E-mail: zhong.wang@mse.gatech.edu.

ORCID

Chaoxing Wu: 0000-0002-1231-2699
Tae Whan Kim: 0000-0001-6899-4986
Zhong Lin Wang: 0000-0002-5530-0380

Author Contributions

‖These authors contributed equally. T.W.K., Z.L.W., and C.W. conceived the project, C.W. and T.W.K. designed and performed the experiments and collected the data. C.W., T.W.K., J.H.P., H.A., J.S., X.C., and Z.L.W. analyzed and discussed the data. All authors discussed the results and contributed to the writing of the manuscript.

Notes

The authors declare no competing financial interest.

ACKNOWLEDGMENTS

This research was supported by the Basic Science Research Program through the National Research Foundation of Korea (NRF) funded by the Ministry of Education, Science and Technology (2016R1A2A1A05005502). C.W. is supported by the Korea Research Fellowship (KRF) Program through the National Research Foundation of Korea funded by the Ministry of Science, ICT, and Future Planning (2015H1D3A1062276).

REFERENCES

(1) Radisavljevic, B.; Radenovic, A.; Brivio, J.; Giacometti, V.; Kis, A. Single-Layer MoS_2 Transistors. *Nat. Nanotechnol.* **2011**, *6*, 147−150.
(2) Lopez-Sanchez, O.; Lembke, D.; Kayci, M.; Radenovic, A.; Kis, A. Ultrasensitive Photodetectors Based on Monolayer MoS_2. *Nat. Nanotechnol.* **2013**, *8*, 497−501.
(3) Tsai, M.-L.; Su, S.-H.; Chang, J.-K.; Tsai, D.-S.; Chen, C.-H.; Wu, C.-I.; Li, L.-J.; Chen, L.-J.; He, J.-H. Monolayer MoS_2 Heterojunction Solar Cells. *ACS Nano* **2014**, *8*, 8317−8322.
(4) Liu, J.; Zeng, Z.; Cao, X.; Lu, G.; Wang, L.-H.; Fan, Q.-L.; Huang, W.; Zhang, H. Preparation of MoS_2-Polyvinylpyrrolidone Nanocomposites for Flexible Nonvolatile Rewritable Memory Devices with Reduced Graphene Oxide Electrodes. *Small* **2012**, *8*, 3517−3522.
(5) Shin, G. H.; Kim, C.-K.; Bang, G. S.; Kim, J. Y.; Jang, B. C.; Koo, B. J.; Woo, M. H.; Choi, Y.-K.; Choi, S.-Y. Multilevel Resistive Switching Nonvolatile Memory Based on MoS_2 Nanosheet-Embedded Graphene Oxide. *2D Mater.* **2016**, *3*, 034002.
(6) Wu, W.; Wang, L.; Li, Y.; Zhang, F.; Lin, L.; Niu, S.; Chenet, D.; Zhang, X.; Hao, Y.; Heinz, T. F.; Hone, J.; Wang, Z. L. Piezoelectricity of Single-Atomic-Layer MoS_2 for Energy Conversion and Piezotronics. *Nature* **2014**, *514*, 470−474.
(7) Zhou, Y.; Liu, W.; Huang, X.; Zhang, A.; Zhang, Y.; Wang, Z. L. Theoretical Study on Two-Dimensional MoS_2 Piezoelectric Nanogenerators. *Nano Res.* **2016**, *9*, 800−807.
(8) Wang, Z. L. Triboelectric Nanogenerators as New Energy Technology for Self-Powered Systems and as Active Mechanical and Chemical Sensors. *ACS Nano* **2013**, *7*, 9533−9557.
(9) Fan, F. R.; Tang, W.; Wang, Z. L. Flexible Nanogenerators for Energy Harvesting and Self-Powered Electronics. *Adv. Mater.* **2016**, *28*, 4283−4305.
(10) Wu, C.; Kim, T. W.; Li, F.; Guo, T. Wearable Electricity Generators Fabricated Utilizing Transparent Electronic Textiles Based on Polyester/Ag Nanowires/Graphene Core−Shell Nanocomposites. *ACS Nano* **2016**, *10*, 6449−6457.
(11) Wang, X.; Wen, Z.; Guo, H.; Wu, C.; He, X.; Lin, L.; Cao, X.; Wang, Z. L. Fully Packaged Blue Energy Harvester by Hybridizing a Rolling Triboelectric Nanogenerator and an Electromagnetic Generator. *ACS Nano* **2016**, *10*, 11369−11376.
(12) Sun, J.-G.; Yang, T. N.; Kuo, I.-S.; Wu, J.-M.; Wan, C.-Y.; Chen, L.-J. A Leaf-Molded Transparent Triboelectric Nanogenerator for Smart Multifunctional Applications. *Nano Energy* **2017**, *32*, 180−186.
(13) Yu, B.; Yu, H.; Wang, H.; Zhang, Q.; Zhu, M. High-Power Triboelectric Nanogenerator Prepared from Electrospun Mats with Spongy Parenchyma-Like Structure. *Nano Energy* **2017**, *34*, 69−75.
(14) Wen, Z.; Chen, J.; Yeh, M. H.; Guo, H.; Li, Z.; Fan, X.; Zhang, T.; Zhu, L.; Wang, Z. L. Blow-Driven Triboelectric Nanogenerator as an Active Alcohol Breath Analyzer. *Nano Energy* **2015**, *16*, 38−46.
(15) Wang, S.; Xie, Y.; Niu, S.; Lin, L.; Liu, C.; Zhou, Y. S.; Wang, Z. L. Maximum Surface Charge Density for Triboelectric Nanogenerators Achieved by Ionized-Air Injection: Methodology and Theoretical Understanding. *Adv. Mater.* **2014**, *26*, 6720−6728.
(16) Xie, Y.; Wang, S.; Niu, S.; Lin, L.; Jing, Q.; Yang, J.; Wu, Z.; Wang, Z. L. Grating-Structured Freestanding Triboelectric-Layer Nanogenerator for Harvesting Mechanical Energy at 85% Total Conversion Efficiency. *Adv. Mater.* **2014**, *26*, 6599−6607.
(17) Chen, J.; Guo, H.; He, X.; Liu, G.; Xi, Y.; Shi, H.; Hu, C. Enhancing Performance of Triboelectric Nanogenerator by Filling High Dielectric Nanoparticles into Sponge PDMS Film. *ACS Appl. Mater. Interfaces* **2016**, *8*, 736−744.
(18) Chandrasekhar, A.; Alluri, N. R.; Saravanakumar, B.; Selvarajan, S.; Kim, S.-J. Human Interactive Triboelectric Nanogenerator as a Self-Powered Smart Seat. *ACS Appl. Mater. Interfaces* **2016**, *8*, 9692−9699.
(19) Xue, F.; Chen, L.; Wang, L.; Pang, Y.; Chen, J.; Zhang, C.; Wang, Z. L. MoS_2 Tribotronic Transistor for Smart Tactile Switch. *Adv. Funct. Mater.* **2016**, *26*, 2104−2109.
(20) Pang, Y.; Xue, F.; Wang, L.; Chen, J.; Luo, J.; Jiang, T.; Zhang, C.; Wang, Z. L. Tribotronic Enhanced Photoresponsivity of a MoS_2 Phototransistor. *Adv. Sci.* **2016**, *3*, 1500419.
(21) Cui, N.; Gu, L.; Lei, Y.; Liu, J.; Qin, Y.; Ma, X.; Hao, Y.; Wang, Z. L. Dynamic Behavior of the Triboelectric Charges and Structural Optimization of the Friction Layer for a Triboelectric Nanogenerator. *ACS Nano* **2016**, *10*, 6131−6138.
(22) Wu, C.; Kim, T. W.; Choi, H. Y. Reduced Graphene-Oxide Acting as Electron-Trapping Sites in the Friction Layer for Giant Triboelectric Enhancement. *Nano Energy* **2017**, *32*, 542−550.
(23) Coleman, J. N.; Lotya, M.; O'Neill, A.; Bergin, S. D.; King, P. J.; Khan, U.; Young, K.; Gaucher, A.; De, S.; Smith, R. J.; Shvets, I. V.; Arora, S. K.; Stanton, G.; Kim, H.-Y.; Lee, K.; Kim, G. T.; Duesberg, G. S.; Hallam, T.; Boland, J. J.; Wang, J. J.; et al. Two-Dimensional Nanosheets Produced by Liquid Exfoliation of Layered Materials. *Science* **2011**, *331*, 568−571.
(24) Wu, C.; Li, F.; Zhang, Y.; Guo, T.; Chen, T. Highly Reproducible Memory Effect of Organic Multilevel Resistive-Switch Device Utilizing Graphene Oxide Sheets/Polyimide Hybrid Nanocomposite. *Appl. Phys. Lett.* **2011**, *99*, 042108.
(25) Eda, G.; Yamaguchi, H.; Voiry, D.; Fujita, T.; Chen, M.; Chhowalla, M. Photoluminescence from Chemically Exfoliated MoS_2. *Nano Lett.* **2011**, *11*, 5111−5116.
(26) Joensen, P.; Frindt, R. F.; Morrison, S. R. Single-layer MoS_2. *Mater. Res. Bull.* **1986**, *21*, 457−461.
(27) Ghatak, S.; Pal, A. N.; Ghosh, A. Nature of Electronic States in Atomically Thin MoS_2 Field-Effect Transistors. *ACS Nano* **2011**, *5*, 7707−7712.
(28) Niu, S.; Wang, S.; Lin, L.; Liu, Y.; Zhou, Y.; Hu, S.; Wang, Y.; Theoretical, Z. L. Study of Contact-Mode Triboelectric Nanogenerators as an Effective Power Source. *Energy Environ. Sci.* **2013**, *6*, 3576−3583.
(29) Wang, S.; Niu, S.; Yang, J.; Lin, L.; Wang, Z. L. Quantitative Measurements of Vibration Amplitude Using a Contact-Mode Freestanding Triboelectric Nanogenerator. *ACS Nano* **2014**, *8*, 12004−12013.

DOI: 10.1021/acsnano.7b03657
ACS Nano XXXX, XXX, XXX−XXX

(30) Yang, Y.; Zhang, H.; Lin, Z.-H.; Zhou, Y. S.; Jing, Q.; Su, Y.; Yang, J.; Chen, J.; Hu, C.; Wang, Z. L. Human Skin Based Triboelectric Nanogenerators for Harvesting Biomechanical Energy and as Self-Powered Active Tactile Sensor System. *ACS Nano* **2013**, *7*, 9213−9222.
(31) Huang, S.; Banerjee, S.; Tung, R. T.; Oda, S. Quantum Confinement Energy in Nanocrystalline Silicon Dots from High-Frequency Conductance Measurement. *J. Appl. Phys.* **2003**, *94*, 7261−7265.
(32) Zhou, Y. S.; Wang, S.; Yang, Y.; Zhu, G.; Niu, S.; Lin, Z.-H.; Liu, Y.; Wang, Z. L. Manipulating Nanoscale Contact Electrification by an Applied Electric Field. *Nano Lett.* **2014**, *14*, 1567−1572.
(33) Wu, C.; Li, F.; Guo, T.; Kim, T. W. Carrier Transport in Volatile Memory Device with SnO_2 Quantum Dots Embedded in a Polyimide Layer. *Jpn. J. Appl. Phys.* **2011**, *50*, 095003.
(34) Mak, K. F.; Lee, C.; Hone, J.; Shan, J.; Heinz, T. F. Atomically Thin MoS_2: A New Direct-Gap Semiconductor. *Phys. Rev. Lett.* **2010**, *105*, 136805.
(35) Streetman, B. G.; Banerjee, S. K. *Solid State Electronic Devices*; Prentice-Hall: Upper Saddle River, NJ, 2000; pp 279−280.

DOI: 10.1021/acsnano.7b03657
ACS Nano XXXX, XXX, XXX−XXX